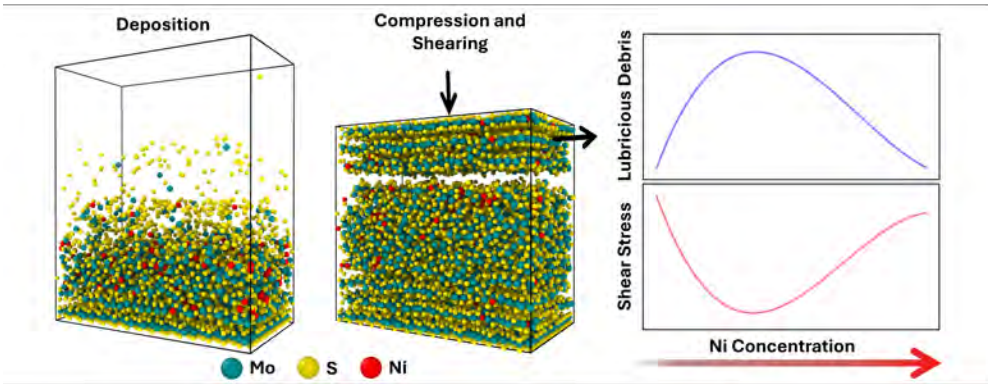

Graphical Abstract

Modeling Sputtering Deposition of MoS_2: Effect of Ni Doping on Nanostructure and Tribological Properties

Sergio Romero Garcia, Abrar Faiyad, Ashlie Martini

Highlights

Modeling Sputtering Deposition of MoS_2: Effect of Ni Doping on Nanostructure and Tribological Properties

Sergio Romero Garcia, Abrar Faiyad, Ashlie Martini

- Sputtering deposition simulations of MoS_2 doped with Ni at different concentrations
- Film morphology analyzed in terms of density, crystallinity, and Ni clustering
- Shear stress lower for sputtered films with intermediate amounts of Ni
- Results explained by the formation of a lubricious particle during shear.

Modeling Sputtering Deposition of MoS_2: Effect of Ni Doping on Nanostructure and Tribological Properties

Sergio Romero Garcia[a], Abrar Faiyad[b], Ashlie Martini[b]

[a]*Department of Materials and Biomaterials Science and Engineering, University of California Merced, 5200 North Lake Rd, Merced, 95343, CA, USA*
[b]*Department of Mechanical Engineering, University of California Merced, 5200 North Lake Rd, Merced, 95343, CA, USA*

Abstract

The nanostructure and tribological properties of molybdenum disulfide (MoS_2) doped with nickel (Ni) were investigated using reactive molecular dynamics simulations. Sputtering deposition simulations captured the formation of MoS_2 films with different Ni concentrations (0%, 2%, 10%, and 15% by weight) and temperatures (300 K and 670 K). The morphology of the deposited films was characterized in terms of density, crystallinity, and Ni clustering. The deposited films were then compressed and sheared in simulations designed to mimic the function of the material as a dry film lubricant. Results showed that, in these simulations, the 2% and 10% Ni-doped films exhibited lower shear stress than the 0% and 15% Ni-doped films. This non-monotonic trend was analyzed in terms of the evolution of the film nanostructure during shear. It was found that the films that exhibited low shear stress formed a lubricious particle, characterized by a crystalline core and amorphous, Ni-containing surface. The lubricious particle was formed through a combination of density, crystallinity, and Ni clustering conditions only possible with the intermediate amount of Ni. The findings suggest that optimizing the Ni concentration distribution during sputtering may be a promising approach to improve the tribological performance of MoS_2 dry film lubricants.

Keywords: MoS_2, Doped MoS2, Molecular Dynamics Simulations, Reactive Simulations, Tribology
PACS: 0000, 1111
2000 MSC: 0000, 1111

1. Introduction

Transition metal dichalcogens (TMDs) are an emerging class of materials with distinctive physical, chemical, and electronic properties. TMDs are two-dimensional materials comprising lamellae of strongly covalent bonded transition metal (e.g., Cr, Mo, W) and chalcogen (e.g., S, Se, Te) atoms stacked and held together by weak van der Waals forces [1, 2]. Molybdenum disulfide (MoS_2) is the most prominent TMD and its abundance on earth and cost effective production methods help position MoS_2 as a promising material for many different applications. [3]. These applications include catalysis [4], electronics [5], and tribology [6, 2].

In tribology, MoS_2 is used as a dry film lubricant (DFL) where liquid lubrication is not ideal. A common example of this is aerospace machinery which must function in conditions ranging from extreme heat to cryogenic temperatures in the vacuum of space. In such environments, the viscosity of liquid lubricants either becomes too low or too high and outgassing is a concern [2]. These issues are overcome by MoS_2 DFLs that have proven effective in providing low friction and long life in harsh environments [7, 8]. However, the effectiveness of MoS_2 DFLs has been reported to be dependent on the method and conditions of synthesis [9].

Methods for synthesizing MoS_2 vary based on the intended use and desired material properties. Techniques such as chemical vapor deposition, molecular beam epitaxy, and metal-organic chemical vapor deposition are favored for electronic applications where crystal quality is paramount [1, 5]. In contrast, sputtering deposition methods are employed for applications where crystal quality is secondary and an amorphous microstructure is acceptable. For tribological applications, sputtering deposition of MoS_2 is the most common method used [10].

The sputtering deposition process involves bombarding a target material with high-energy ions, causing atoms to condense on a substrate, forming a thin film [11]. Physical characterization of sputtered thin films has led to better understanding of growth morphology [12, 13], substrate effects [14], and correlations between process conditions and microstructure-dependent physical or electronic properties [15]. For example, a comparison of MoS_2 thin films deposited at room temperature and 670 K showed that the room temperature films had an amorphous smooth structure while the films deposited at 670 K were nano-crystalline with a grained surface morphology [15]. The microstructure of a sputter deposited MoS_2 directly affects its properties and

performance as a DFL [12, 16]. Consequently, various methods have been proposed to enhance the final film structure, including laser annealing, vacuum heat treatment, and co-sputtering with other elements.

Co-sputtering MoS_2, also referred to as doping, has been shown to enhance MoS_2 DFL tribological properties in both vacuum and ambient conditions. Dopants can substitute the Mo or S atoms in the MoS_2 lamella or remain intercalated between layers [2]. The mechanisms by which dopants enhance the tribological properties of MoS_2 is a topic of active research. Increased density [17, 18, 19] and increased hardness [20, 21, 16, 22, 23, 13] are two widely cited mechanisms. However, the increase of hardness is not a universal. Some dopants reduce the hardness of the DFL and still improve its tribological properties by facilitating transfer film formation [24, 22, 25]. Various dopants have previously been evaluated, including titanium [26], gold [25], and nickel [27]. Particularly, nickel (Ni) has been considered for doping MoS_2 due to its relative abundance, ionic radius similar to Mo, and electron configuration [28]. Computational studies showed that Ni intercalated between MoS_2 lamella can increase inter-layer binding and atomic roughness which reduces the work of adhesion and contact area [29, 30]. Ni-doped MoS_2 DFLs typically have Ni concentrations ranging from 2% to 15% by weight [31, 10]. It has been reported that the concentration of Ni can influence the wear resistance and electrical conductivity of the material [27, 32, 33, 34]. However, the effect of Ni concentration on structural variations in sputtered films and the resultant DFL performance is not fully understood.

This limited understanding is partially due to the challenges associated with using experimental methods to monitor film growth during sputtering or film evolution during use as a DFL. However, experiments can be complemented by computational methods such as molecular dynamics (MD) simulations to identify the atomistic origins of correlations between processing parameters and material properties. For MoS_2 films specifically, MD simulations have previously been instrumental in explaining the effects of parameters such as temperature [35], oxidation [36], and shear stress [37, 7, 38, 39], on the mechanical properties and nano-structure of MoS_2. For processes that involve the formation and breaking of chemical bonds, ReaxFF potentials have been developed for MoS_2 [40, 41, 42]. These potentials have been used to simulate processes including the crystallization of MoS_2 from amorphous precursors [43, 44], demonstrating the robustness of reactive MD simulations in investigating MoS_2 at an atomic scale.

To simulate sputtering deposition, methods have been developed to model the process as a constant flux of atoms introduced randomly into the simulation box, with depositing atoms traveling toward the substrate at a defined velocity [45]. This simulation strategy has proven successful in modeling deposition of various materials, including silicon dioxide [46, 47, 48] and gold clusters [49]. The recent development of a new ReaxFF potential that includes parameters for interactions between Ni, Mo, and S enabled simulations of sputtering deposition of Ni-doped MoS_2 [42]. The results showed the formation of a thin, primarily amorphous film formed by sputtering [42]. However, no analysis of the Ni distribution in the material and its effect on the film nano-structure was performed. Similarly, the effects of Ni concentration on nano-structure and the tribological properties of the deposited material were not explored.

In this study, we conducted reactive MD simulations to model the deposition of MoS_2 films. The objective was to investigate how processing variables influence the nano-structure and material properties of the deposited films which, in turn, affect its performance as a DFL. Analyses of the deposited films included assessing the density, crystallinity, and Ni distribution of the films at varying Ni concentrations and two different temperatures. Then, we conducted simulations of sliding [50] to evaluate frictional behavior and the evolution of the material in response to shear. The results provide a better understanding of how the deposition conditions and Ni doping affect the performance and characteristics of MoS_2-based DFLs.

2. Methods

Reactive MD simulations were performed using the ReaxFF potential with parameters developed for Ni-doped MoS_2 [42] with a time step of 0.25 fs. All simulations were run using LAMMPS, atom configurations were visualized with OVITO, and post-processing was done with custom Python scripts. Fig. 1 shows representative snapshots at different stages of the simulation process including deposition, equilibration of the deposited material, followed by compression and shear to mimic a DFL in use.

Sputtering deposition simulations were performed using the NVE ensemble with the Berendsen thermostat [51] with a damping parameter of 10 fs. The simulation box was $8.2 \times 4.5 \times 10.0$ nm in the x-, y-, and z-directions, respectively, with periodic boundary conditions in the x- and y-directions. Atoms with vertical positions between 0 and 0.2 nm were fixed throughout

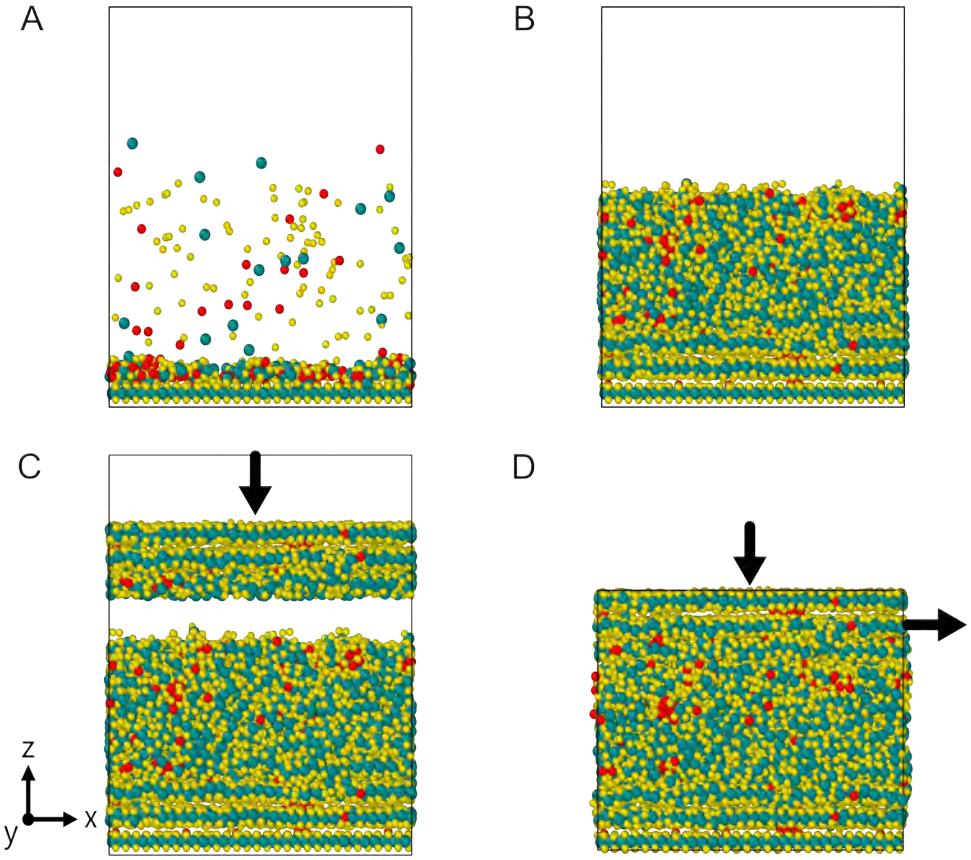

Figure 1: Snapshot representations of the simulations steps: (A) sputtering deposition, (B) equilibration, (C) compression, and (D) shearing of the 300 K, 10% Ni doped MoS_2 thin film. Red, yellow, and green spheres represent Ni, S, and Mo atoms, respectively

the simulation. A Lennard-Jones virtual wall was used to prevent atoms from crossing the boundary area at the top edge of the simulation box.

The initial configuration was a substrate of one MoS_2 sheet built using VESTA [52]. The atoms above 0.2 nm were subject to energy minimization and equilibration at the deposition temperature. Next, Mo, S, and Ni atoms were continuously deposited into the simulation box from a height of 7.0 nm above the substrate surface. The deposition ratios used, shown in Table S1, were based on concentrations reported from X-ray photoemission spectroscopy (XPS) data of MoS_2 Ni-doped at 0, 2, 10, and 15 % by weight [31]. Deposition rates for Mo or Ni were one atom every 40 fs with

deposition energies of 10 eV; for S atoms, the deposition rate was one atom every 20 fs with a deposition energy of 0.5 eV. The deposition temperatures were 300 K and 670 K. Following previous simulations of deposition [47], a reflective virtual wall was placed above the substrate to reflect S atoms (deposited at lower energy) that initially did not remain in the film back downward. The reflective wall started at a z-position of 4.8 nm and then moved upward at a velocity of 2.5 nm/ns as the film grew to a final z-position of 5.5 nm. A snapshot of the 300 K, 10% Ni system after 0.01 ns of deposition is shown in Fig. 1(A). Deposition continued until 8,100 atoms were deposited.

After deposition, the reflective virtual wall was removed and deposited films were equilibrated for 0.75 ns at the simulation temperature for a total simulation time of 1 ns. This duration was determined to be long enough based on the mean density of the film which was found to reach a steady-state value at around 0.25 ns after deposition. A snapshot of the 300 K deposition with 10% Ni after the equilibration process is shown in Fig. 1(B). After equilibration, any unbonded S atoms were removed from the system in preparation for compression and shearing simulations.

To study the tribological properties of the sputter deposited MoS_2 thin films, a shearing protocol was implemented for the four different Ni percentage cases sputtered at 300 K. First, a counter surface was constructed from the bottom of the previously sputter deposited film (the bottommost 2.1 nm of the model, approximately three layers of MoS_2). This counter surface was rotated by 180°and then placed 1 nm above the deposited film, as shown in Fig. 1(C). The new model, containing both the deposited film and counter surface, was minimized using conjugate gradient method. In the newly created simulation cell, the atoms in the top 0.31 nm were treated as a rigid body and the atoms in the bottom 0.31 nm were fixed. The system was equilibrated in an NVT ensemble at 300 K temperature for 100 ps.

Next, a 5 GPa pressure was applied to the top rigid layer, moving it downward in the z-direction towards the deposited material. The system was compressed for for 200 ps until the height of the center of mass of the top rigid body reached steady state. Finally, while maintaining a pressure of 5 GPa, a velocity of 50 m/s was applied to the top rigid body in the x-direction, as shown in Fig. 1(D). The total simulation time for the sliding step was 2.5 ns. During sliding simulation, the shear force in the x-direction on upper rigid wall was calculated and averaged every 5 ps. Shear stress was then calculated from the average shear force divided by the x-y cross-sectional area of the simulation cell.

3. Results and Discussion

3.1. Sputtering Deposition

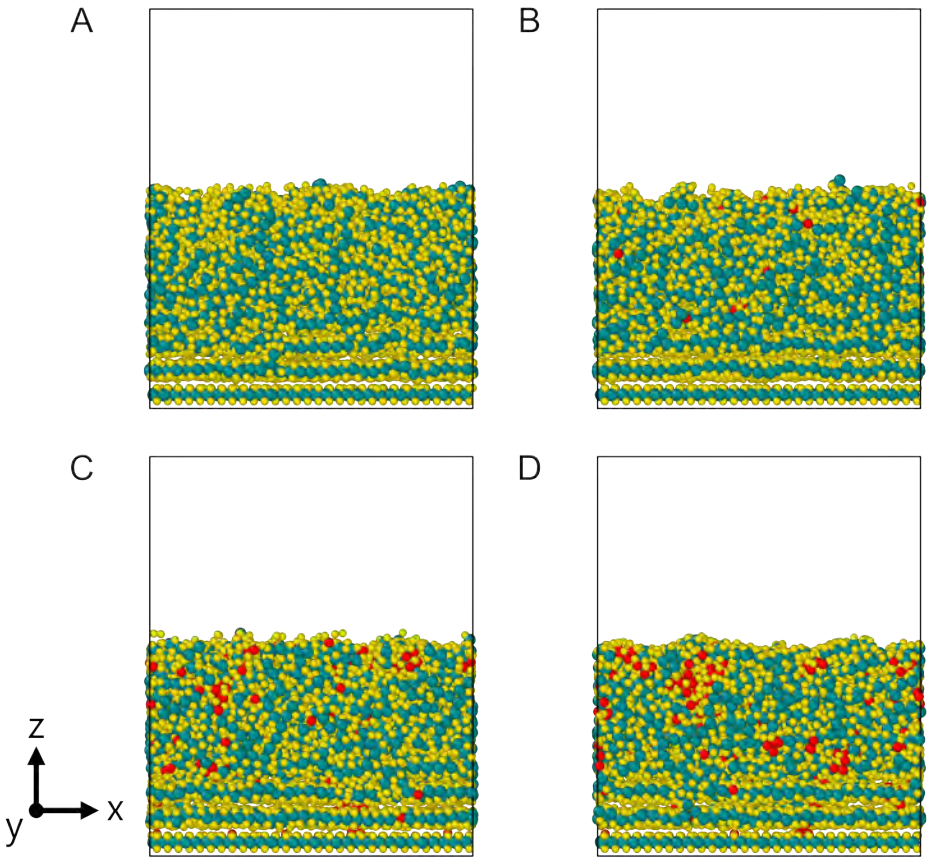

Figure 2: Snapshot representations of (A) undoped, (B) 2 % Ni doped, (C) 10 % Ni doped, and (D) 15 % Ni doped MoS_2 depositions at 300 K after equilibration.

Snapshots of the model systems after 300 K deposition and equilibration are shown in Fig. 2. In all four cases, there was visual evidence that the degree of crystallinity of the material decreased with increasing distance from the bottom MoS_2 layer onto which the atoms were deposited. Also, comparing the three doped films, there appeared to be clustering of Ni atoms in the higher Ni concentration cases. Similar visual trends were observed from the 670 K deposition simulations, shown in Fig. S1. The density, crys-

tallinity, and Ni clustering in the films were quantified and compared across the different temperature and Ni concentration cases.

First, the density of the films was evaluated. Density was calculated as a function of vertical position by dividing the simulation cell into 0.6 nm thick bins, as shown in Fig. S3(A). Steady state density was calculated from the mass of the atoms in each bin divided by the bin volume, averaged over the last 0.5 ns of the deposition simulations. The results in Fig. 3 show the highest density near the substrate for all temperatures and Ni percentage cases. The density decreased farther from the substrate, consistent with observations in a previous experimental study of MoS_2 films [53].

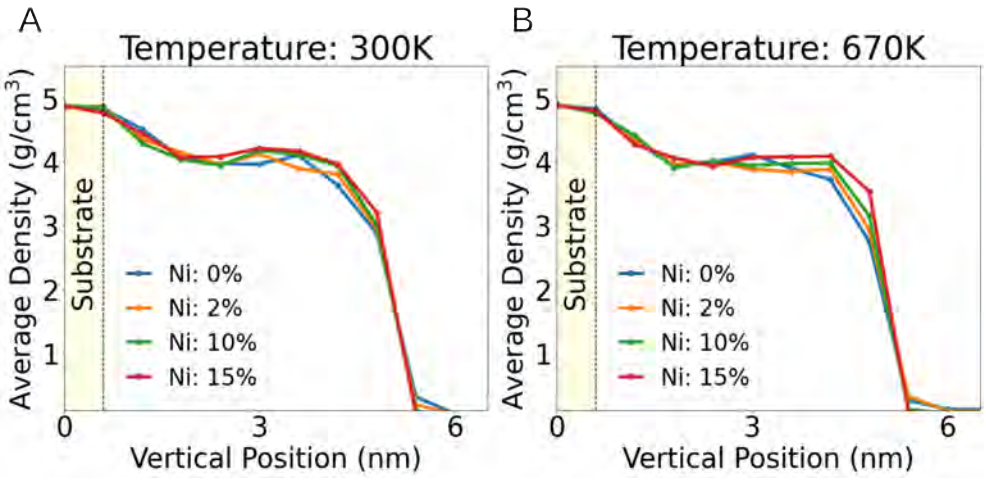

Figure 3: Time-averaged density with respect to vertical position for all Ni percentage deposited films at (A) 300 K and (B) 670 K.

In the bulk of the film (between 2.0 and 4.0 nm), there was no statistically significant difference between the average densities at the various temperature and Ni percentage cases, with an average density across all cases of 3.98 $\pm$ 0.07 g/cm^3. Previous experimental studies reported a density of 4.3 g/cm^3 [15] which is slightly larger than that calculated in the bulk of the simulated film. The difference in density is likely due to the short time scale of the simulations which does not allow for complete densification of the film. Regardless, the analysis of film density suggested that subsequent characterization of the deposited films should focus on the region between 2.0 and 4.0 nm.

Visual analysis of the material evolution with time (shown for the 300K,

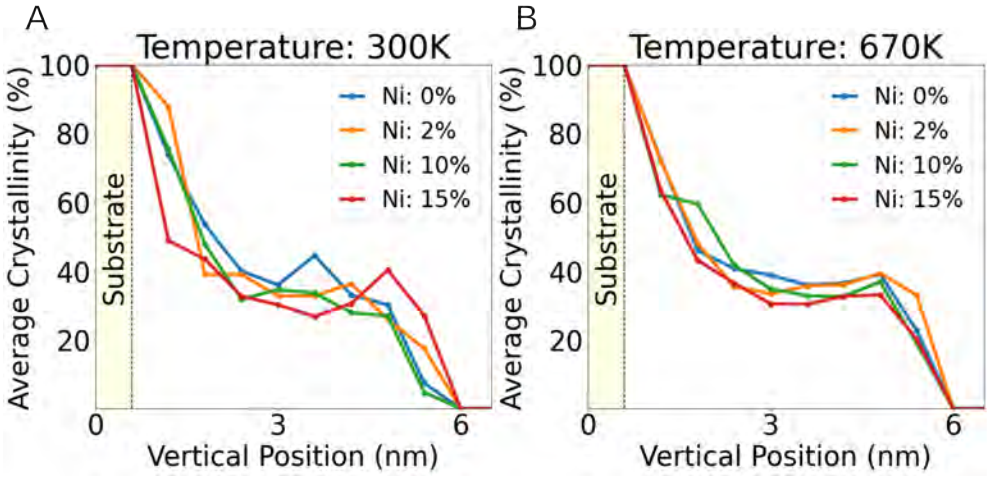

Figure 4: Time-averaged crystallinity with respect to vertical position for all Ni percentage deposited films at (A) 300 K and (B) 670 K.

10 % Ni doped case in Fig. S4(A)) indicated that the deposited material contained both amorphous and crystalline regions. The binning approach described above for calculating density was implemented to quantify the crystallinity of the material based on Mo and S bond distances and angles [43]. Briefly, Mo atoms with six bonded neighbors (S in the undoped system and S or Ni in the doped systems) were identified. Then, the angle between each of those Mo atoms and its neighbor atoms (Neighbor-Mo-Neighbor) was calculated. The angles were compared to ranges provided in literature [43] to identify atoms in an MoS_2 crystal structure. Finally, the crystallinity percentages were calculated from the number of Mo in a crystal configuration divided by the total number of Mo atoms in the bin. Crystallinity as a function of vertical position averaged over the last 0.5 ns of equilibration is shown in Fig. 4(A) and (B).

Similar to the density trend, the highest crystallinity occurred in the material deposited directly on the substrate and then crystallinity decreased with increasing distance. It has been reported that the microstructure of sputtered deposited materials is influenced by the substrate lattice structure [54]. In our case, the ideal crystal lattice of the substrate acted as a template that facilitated the formation of highly crystalline material at the deposition-substrate interface. The difference between the average crystallinity of the bulk film between 2.0 and 4.0 nm was not significant for the

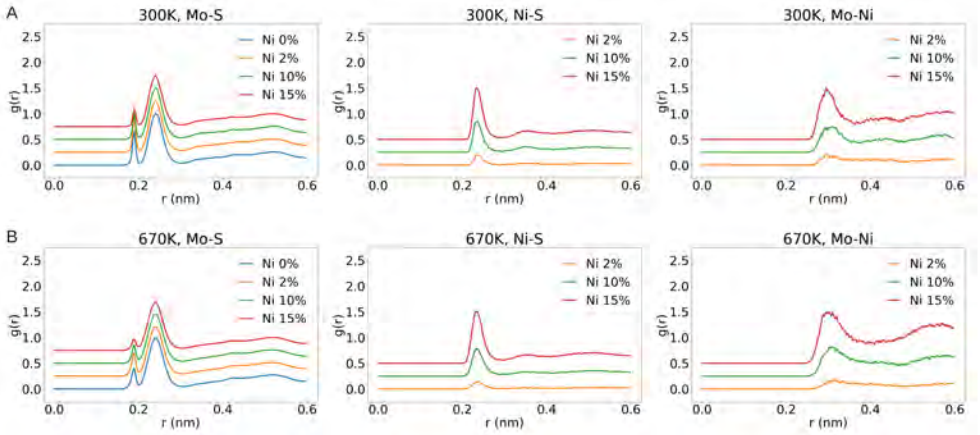

Figure 5: Radial distribution function analysis for Mo-S, Ni-S, and Mo-Ni atom pairs at (A) 300 K and (B) 670 K.

different temperature or Ni concentration cases (Table S2 and Fig. S4(B)) and the mean bulk crystallinity for all cases was 35% ± 3%.

To further analyze the influence of temperature and Ni on crystal formation and nanostructure, we calculated radial distribution functions (RDFs) of the Ni-S, Mo-S, and Mo-Ni atom distances after 0.5 ns of equilibration, as shown in Fig. 5. The positions of the peaks for Mo-S and Ni-S atom distances were the same at both temperatures and, for Ni-S, the same at all three Ni percentages. However, for Mo-Ni atom distances, there was some difference between the cases for the second peak, which appeared around 0.55 nm (at the same position as the second peak in the Mo-S RDFs). This peak was more prominent at 670 K compared to 300 K and for the higher Ni concentration cases (10 % and 15 %). This observation indicated a more ordered arrangement of Mo-Ni atoms in films deposited at higher temperatures which may be explained by more sulfur vacancies in the higher energy conditions [55] that could then be occupied by Ni atoms.

It has been reported that, during co-sputtering of MoS_2 Ni films, Ni is dispersed in small disordered clusters that influence the film growth [56]. Fig. S5 shows snapshot representations of the Ni atoms at the end of equilibration where some clustering is observed, particularly at the higher Ni percentage cases. To quantify this, Ni cluster size was defined based on number of Ni atoms bonded to one another and tracked over time for each temperature and Ni percentage case. Analysis of Ni clustering as a function of time showed

that the cluster sizes were relatively constant after about 0.5 ns (Fig. S6).

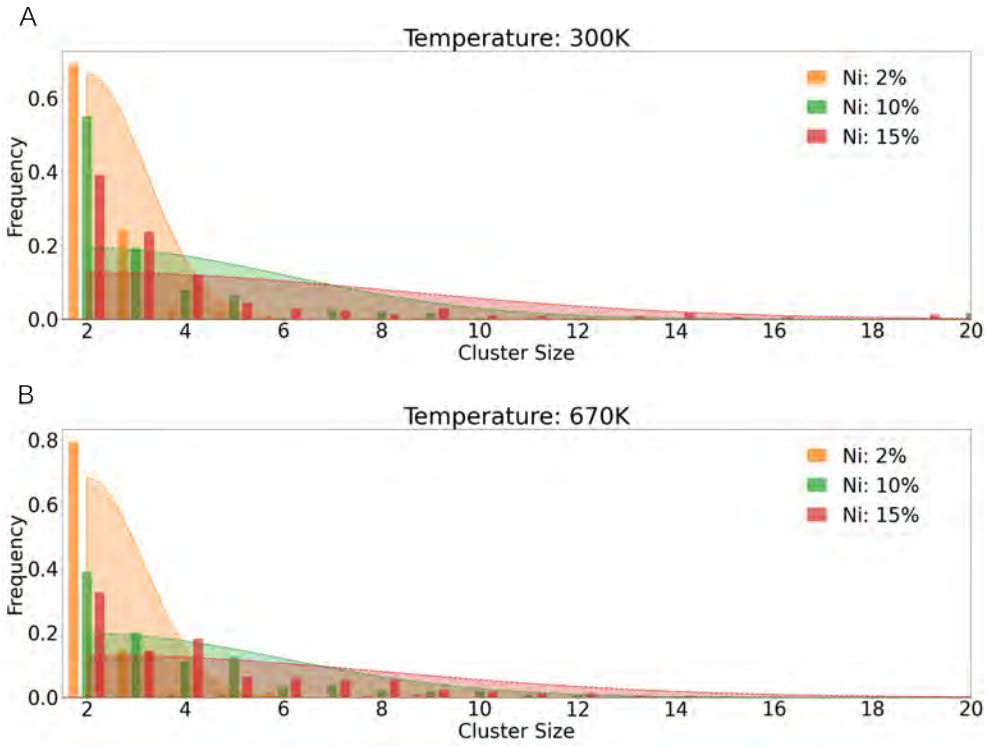

Figure 6: Distributions of Ni cluster sizes for deposition at (A) 300 K and (B) 670 K. Shaded regions correspond to skewed distributions fitted to the cluster size data.

The distributions of steady-state cluster sizes (quantified by number of Ni atoms per cluster) are shown in Fig. 6(A) and (B). The histograms were fitted to skewed probability density functions to better visual the differences between the different cases. The mean cluster sizes at temperatures 300 K and 670 K were 2.26 and 2.15 for 2% Ni, 3.37 and 3.94 for 10% Ni, and 4.83 and 5.30 for 15% Ni, respectively. Although the mean cluster size was slightly larger at the higher temperature for the 10% and 15% cases, the effect of temperature was minimal compared to that of Ni concentration. At either temperature, the size of Ni clusters increased with Ni concentration.

3.2. Compression and Shear

The equilibrated MoS_2 coatings from the 300 K deposition simulations were confined, compressed, and sheared. The shear stress on the top layer

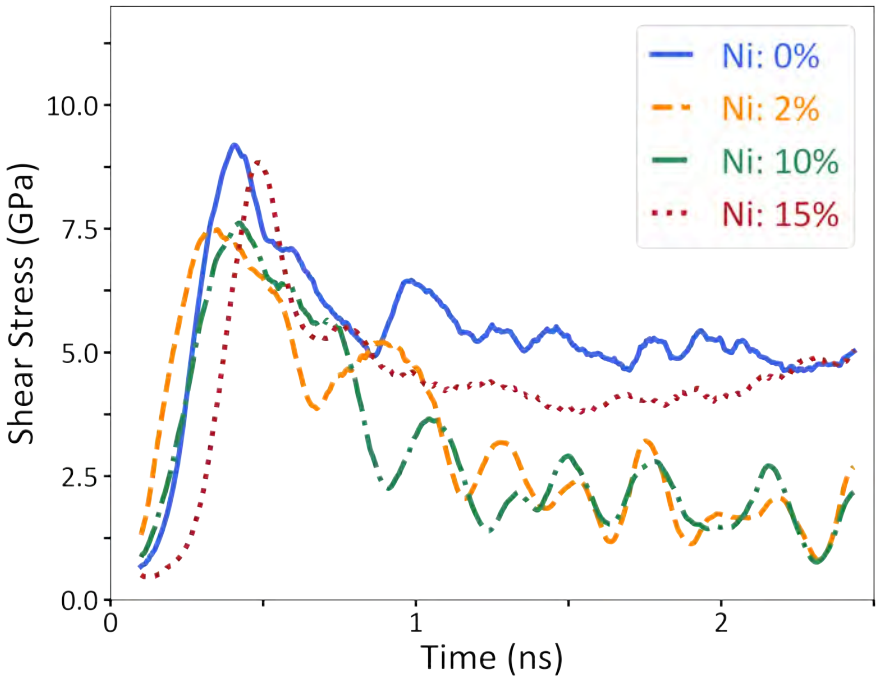

Figure 7: Evolution of shear stress during shearing of films sputter deposited at 300 K.

during the shearing stage is shown in Fig. 7. During the run-in period, all films showed an initial steep increase in the shear stress followed by a gradual decrease before converging towards a steady state value. This run-in behavior can be explained by the evolution of density, crystallinity, Ni distribution, and wear particle formation, as discussed later. The shear stress in the four cases studied fluctuated about a steady-state value after approximately 1.25 ns of sliding.

The average shear stress in steady state for the particular cases studied was 5.0 GPa for 0%, 1.9 GPa for 2%, 2.0 GPa for 10%, and 4.3 GPa for 15%. The shear stress was highest for the undoped coating, indicating the Ni was beneficial to the material as a DFL. Higher shear stress implies faster removal of coating material, so the simulation shear stress trends are consistent with results from previous experimental studies that showed the wear life of 7% Ni doped MoS_2 films was longer than that of undoped MoS_2

at low contact pressures. [27] Interestingly, in Fig. 7, the steady-state shear stress does not vary monotonically with Ni concentration. This has been reported experimentally in Ni-doped MoS_2 films where friction was reported to increase when Ni doping exceeded 10% [32] or 11% [18] Ni by weight.

Visual analysis of the dynamic evolution of the material structure during shearing (Fig. S7) indicated different sliding mechanisms for the different cases. Particularly, for the cases studied, the 2 % and 10 % Ni doped films exhibited the formation of a wear particle or debris. The formation of wear debris significantly affected the sliding mechanism and resulted in the low friction behavior of the coating. It has been proposed previously that MoS_2 DFLs function through a mechanism involving the formation of lubricious wear particles [57, 27, 58, 59]. These particles are believed to form during run-in and provide lubrication. Although the simulations cannot capture wear because of the periodic nature of the model, the formation of particles or debris can be seen. Fig. 8 shows snapshots of the four model systems with the atoms colored based on their lateral displacement. In the cases that lowest shear stresses were exhibited in our set of simulations, 2% and 10% Ni, there is visual evidence of a particle that contains atoms with displacement between that of the top wall and the lower half of the coating, indicating this particle is accommodating most of the shear.

To quantify these observations, the distribution of density in the material over time was calculated for each Ni percentage case, as shown in Fig. 9. In all four cases, the highest density was just above the substrate (around 2.5 nm) and the density of this region increased after the initial 0.5 ns of sliding in all cases. Also, for the 2% and 10% Ni doped films (Fig. 9(B) and (C)), starting around 1 ns, there was a density drop at vertical positions between 4 and 6 nm which was attributable to the fact that this region contained the wear particle with high mobility, as seen in Fig. 8. For these two cases, the density of the top half of the films oscillated over time, which could be linked to the large fluctuations of shear stress observed in Fig 7 after 1 ns of shearing.

Complementing the density observations, crystallinity was tracked during shear. Like density, the crystallinity of the material evolved over time and was vertical position dependent, as shown in Fig. 10. In all four cases, the initially crystal rich regions became more amorphous after the initial few hundreds of ps of sliding. After this run-in stage, the crystallinity distribution of the coatings changed little with subsequent sliding. In the 0% and 15% Ni cases, there were regions of higher crystallinity around 1 nm and then again around 3.5 nm. Above that, there was a region of amorphous material

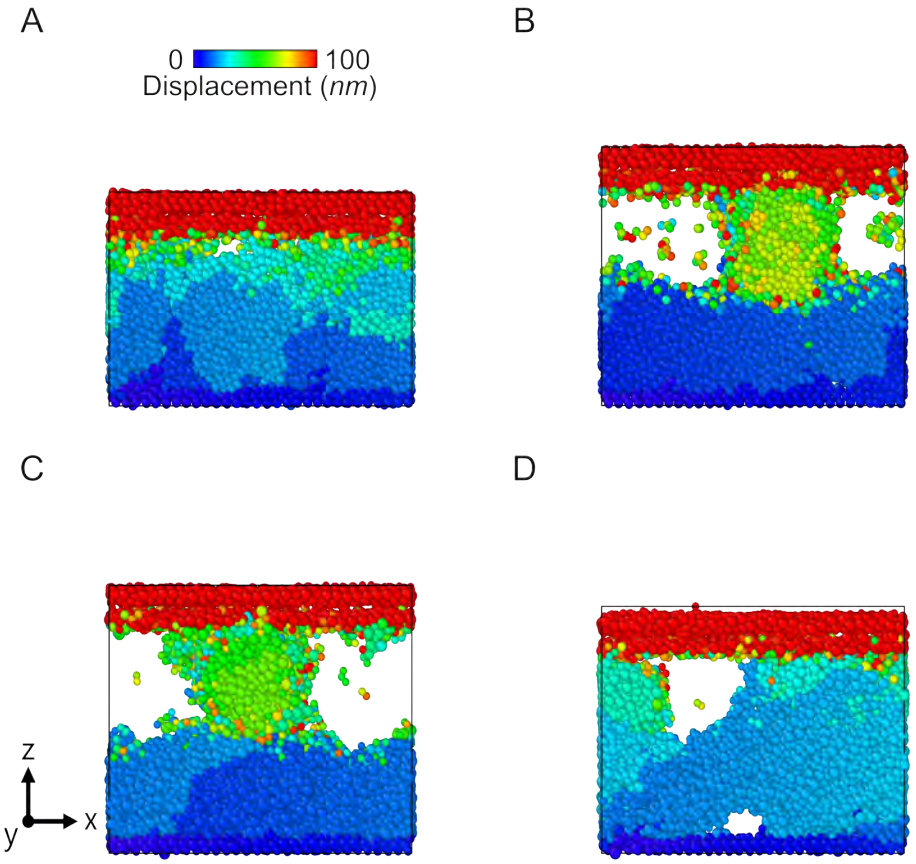

Figure 8: Snapshot representation of (A) 0%, (B) 2 %, (C) 10%, and (D) 15% Ni-doped films during shearing at time 2.4 ns. The color represents the x-direction displacement magnitude of the atoms.

corresponding to the location where most of the shear was accommodated. For the 2 % and 10 % Ni doped cases, the upper half of the coating was more amorphous than the lower half. The top amorphous region corresponded to the position of the lubricious particle. The crystallinity of the wear particles specifically was analyzed for the 2% and 10% cases. As shown in Fig S8, the lubricious particles comprised more crystalline material in the core with primarily amorphous surfaces.

Finally, the Ni-cluster size evolution over time during shear is shown in Fig. 11. During the simulation run-in period, some of the larger clusters formed during the deposition were broken into smaller clusters. Despite

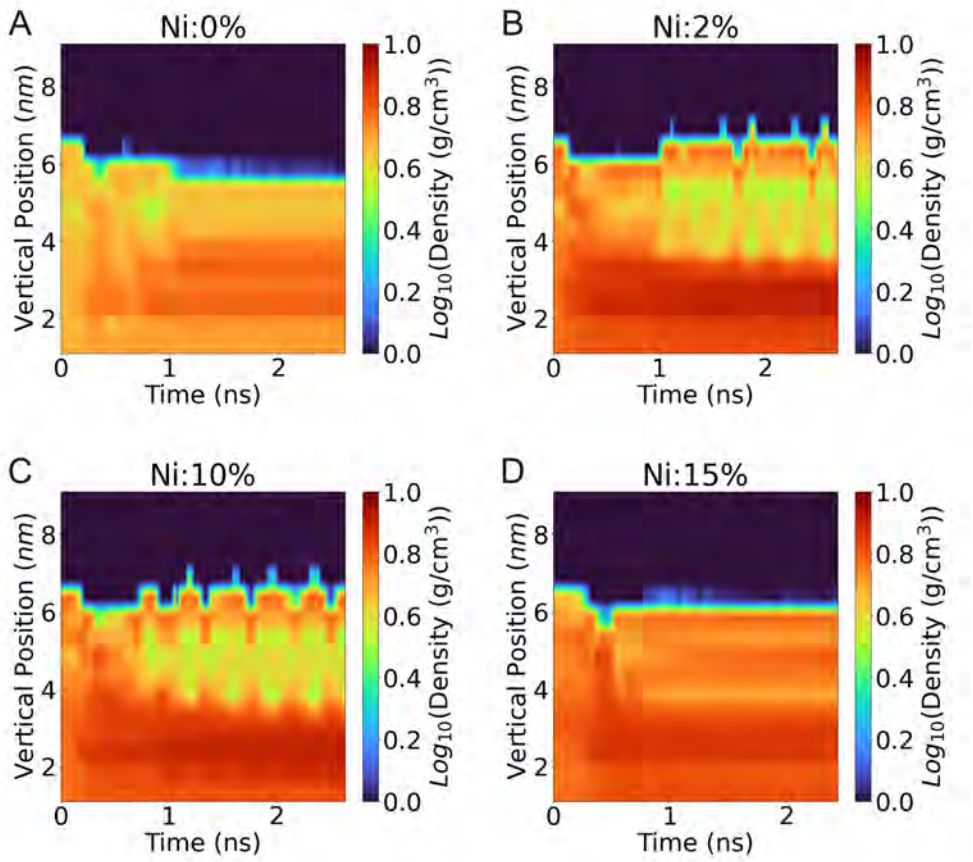

Figure 9: Evolution of density as a function of vertical position and time for the shearing simulations (after compression is complete) with color map representing the log of the density for (A) 0 %, (B) 2%, (C) 10%, and (D) 15% Ni doped MoS_2 films.

the decreased cluster size, the trend observed during deposition, i.e., that higher Ni concentration corresponded to larger clusters, was also observed throughout shearing. For all three cases, the majority of the clusters present during steady-state consisted of single digit Ni atoms with mean cluster sizes of 2.3, 3.1, and 4.2 for 2%, 10%, and 15% Ni-concentrations, respectively. The distribution of the Ni in the lubricious particles formed in the 2% and 10% cases was analyzed visually and, as shown in Fig S9, the Ni atoms were present primarily at near the surface of the particles as opposed to in the core.

The above analysis corroborates previous work that proposed MoS_2 DFLs

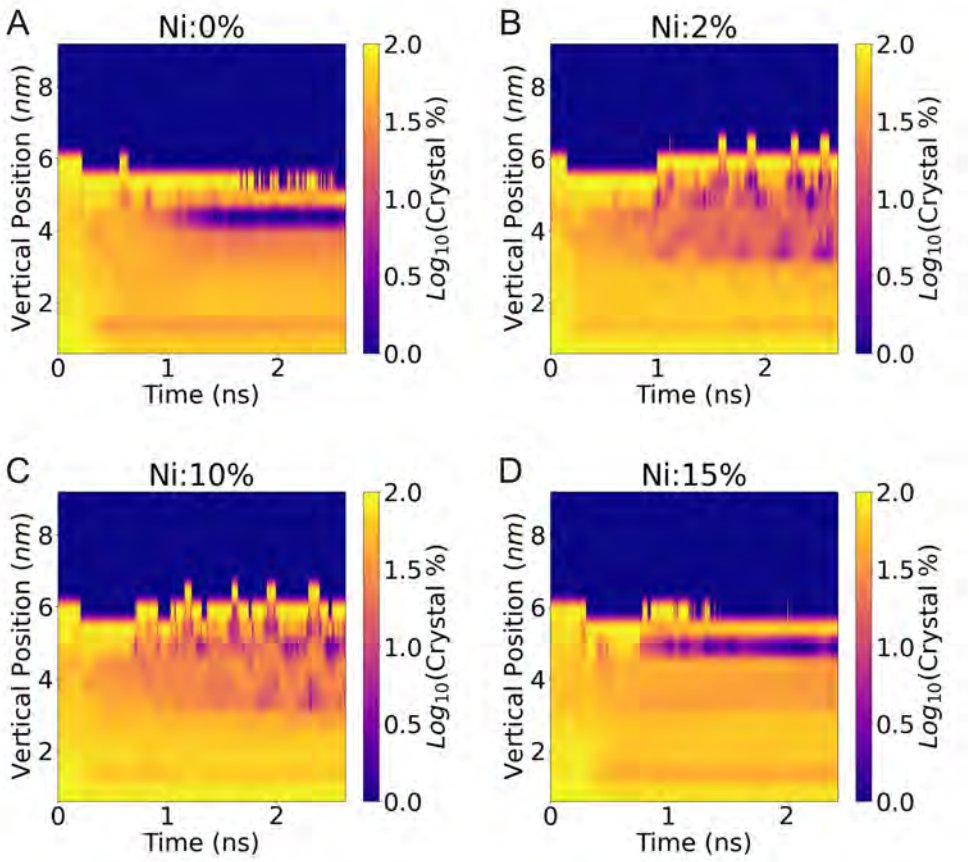

Figure 10: Evolution of crystallinity as a function of vertical position and time during shearing simulations with color map representing the log of the percent crystalline material for (A) 0 %, (B) 2%, (C) 10%, and (D) 15% Ni doped MoS_2 films.

lubricate, at least in part, through the formation of lubricious wear particles [57, 27, 58]. The observation that Ni affects the formation of lubricious debris in simulations may also provide a possible explanation for previous experimental studies that reported a non-monotonic relationship between Ni concentration and DFL performance [32, 18] (Ni has also been reported to affect hardness [18, 60, 32], although that is not something can be directly quantified in these simulations). The remaining question is how Ni can affect the formation or lubricity of wear particles. In the simulations of 2% and 10% Ni, the wear particles were more crystalline in the center and Ni atoms were primarily present in the amorphous surface as shown in Fig. S8. This

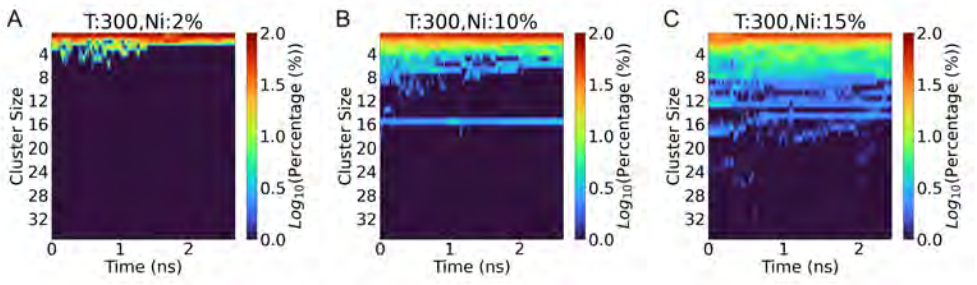

Figure 11: Abundance plot of the evolution of Ni cluster sizes over time during shearing simulations with color map representing the log of the Ni cluster size (number of Ni atoms) for (A) 2 %, (B) 10%, and (C) 15%.

implies that lubricious particles might be less likely to form when there is no Ni available because of the strong bonds between Mo and S facilitate crystallinity and inhibit the formation of distinct particles, i.e., no Ni is available to separate the particle from the bulk of the film. Also, lubricious particles might not form with too much Ni because large and prevalent Ni clusters could impede the formation of a crystalline particle core. Although we did not simulate higher Ni concentrations, the results indicate that adding more Ni would be even more detrimental to the formation of lubricious particles and adversely affect shear stress.

4. Conclusions

In this study, the effect of Ni dopant percentages on the nanostructure and tribological properties of sputtered deposited MoS_2 was investigated using reactive molecular dynamics simulations.

A sputtering deposition simulation procedure was implemented to form DFLs with different Ni concentration. Characterization of the resulting films showed that crystal percentage and density varied across the material vertically, with the highest density and crystallinity observed in the deposited material just above the MoS_2 substrate. Neither temperature nor Ni concentration had a statistically significant effect on density and crystallinity in the bulk of the simulated films. In the cases with Ni dopant, it was found that the Ni formed clusters with a range of sizes and that larger clustered could be formed with higher Ni concentrations. The difference between the nanostructures of the films deposited at 300 and 670 K was minimal and seen only as more long-range ordering of the Mo and Ni atoms in the material.

Shearing simulations for the sputtered DFL deposited at 300 K. The results showed that Ni dopants at 2% and 10% had lower shear stress at steady state than that for Ni dopants at 0% and 15%. Further investigation of the density, crystallinity and Ni-clustering during shearing showed the formation of the lubricious wear particles for the 2% and 10% films. These particles were found to be more crystalline in the core with amorphous and Ni-containing surface material. In the simulations reported here, this combination of crystallinity and dopant concentration was only possible with the intermediate amounts of Ni in the film.

The findings of this study reveal a mechanism by which Ni dopants can improve the performance of an MoS_2 DFLs. It is important to note that the optimum Ni percentages identified here may be specific to this simulation set up. However, the finding that Ni dopants can affect the formation of lubricious wear debris is generally applicable and provides a possible explanation for the non-monotonic dependence of tribological properties on dopant concentration. Awareness of this mechanism may guide future experiments that directly measure concentration dependence for Ni as well as other dopants. Finally, the modeling approach developed here might be leveraged to further understand and then improve the performance of these materials.

5. Acknowledgements

Simulations run on resources provided by the ACCESS advanced computing and data resource supported by the National Science Foundation. Part of this research was conducted using Pinnacles (NSF MRI, # 2019144) at the Cyberinfrastructure and Research Technologies (CIRT) at University of California, Merced.

References

[1] S. Manzeli, D. Ovchinnikov, D. Pasquier, O. V. Yazyev, A. Kis, 2D transition metal dichalcogenides, Nat. Rev. Mater. 2 (8) (2017) 17033.

[2] M. R. Vazirisereshk, A. Martini, D. A. Strubbe, M. Z. Baykara, Solid lubrication with MoS2: A review, Lubricants 7 (7) (2019) 57.

[3] K.-Q. Lu, M.-Y. Qi, Z.-R. Tang, Y.-J. Xu, Earth-abundant MoS2 and cobalt phosphate dual cocatalysts on 1D CdS nanowires for boosting

photocatalytic hydrogen production, Langmuir 35 (34) (2019) 11056–11065.

[4] M.-R. Gao, M. K. Y. Chan, Y. Sun, Edge-terminated molybdenum disulfide with a 9.4-Å interlayer spacing for electrochemical hydrogen production, Nat. Commun. 6 (1) (2015) 7493.

[5] N. Choudhary, M. D. Patel, J. Park, B. Sirota, W. Choi, Synthesis of large scale MoS2 for electronics and energy applications, J. Mater. Res. 31 (7) (2016) 824–831.

[6] M. R. Hilton, R. Bauer, P. D. Fleischauer, Tribological performance and deformation of sputter-deposited MoS2 solid lubricant films during sliding wear and indentation contact, Thin Solid Films 188 (2) (1990) 219–236.

[7] P. Serles, K. Gaber, S. Pajovic, G. Colas, T. Filleter, High temperature microtribological studies of MoS2 lubrication for low earth orbit, Lubricants 8 (4) (2020) 49.

[8] J. F. Curry, N. Argibay, T. Babuska, B. Nation, A. Martini, N. C. Strandwitz, M. T. Dugger, B. A. Krick, Highly oriented MoS2 coatings: Tribology and environmental stability, Tribol. Lett. 64 (1) (2016) 11.

[9] S. Das, M. Kim, J.-W. Lee, W. Choi, Synthesis, properties, and applications of 2-D materials: A comprehensive review, Crit. Rev. Solid State Mater. Sci. 39 (4) (2014) 231–252.

[10] I. Efeoglu, Sputtering MoS2-based coatings, in: Encyclopedia of Tribology, Springer US, Boston, MA, 2013, pp. 3233–3252.

[11] V. Buck, Preparation and properties of different types of sputtered MoS2 films, Wear 114 (3) (1987) 263–274.

[12] R. Bichsel, P. Buffat, F. Levy, Correlation between process conditions, chemical composition and morphology of MoS2films prepared by RF planar magnetron sputtering, J. Phys. D Appl. Phys. 19 (8) (1986) 1575–1585.

[13] H. Li, X. Li, G. Zhang, L. Wang, G. Wu, Exploring the tribophysics and tribochemistry of MoS2 by sliding MoS2/ti composite coating under different humidity, Tribol. Lett. 65 (2) (2017) 38.

[14] V. J. Cicily Rigi, M. K. Jayaraj, K. J. Saji, Effect of substrate and substrate temperature on the deposition of MoS2 by radio frequency magnetron sputtering, J. Vac. Sci. Technol. A 40 (3) (2022) 032201.

[15] R. Kaindl, B. C. Bayer, R. Resel, T. Müller, V. Skakalova, G. Habler, R. Abart, A. S. Cherevan, D. Eder, M. Blatter, F. Fischer, J. C. Meyer, D. K. Polyushkin, W. Waldhauser, Growth, structure and stability of sputter-deposited MoS2 thin films, Beilstein J. Nanotechnol. 8 (2017) 1115–1126.

[16] D. G. Teer, New solid lubricant coatings, Wear 251 (1-12) (2001) 1068–1074.

[17] J. R. Lince, Doped MoS2 coatings and their tribology, in: Encyclopedia of Tribology, Springer US, Boston, MA, 2013, pp. 782–785.

[18] J. S. Zabinski, M. S. Donley, S. D. Walck, T. R. Schneider, N. T. Mcdevitt, The effects of dopants on the chemistry and tribology of sputter-deposited MoS2Films, Tribol. Trans. 38 (4) (1995) 894–904.

[19] T. F. Babuska, J. F. Curry, M. T. Dugger, P. Lu, Y. Xin, S. Klueter, A. C. Kozen, T. Grejtak, B. A. Krick, Role of environment on the shear-induced structural evolution of MoS2 and impact on oxidation and tribological properties for space applications, ACS Appl. Mater. Interfaces 14 (11) (2022) 13914–13924.

[20] A. A. Tedstone, D. J. Lewis, P. O'Brien, Synthesis, properties, and applications of transition metal-doped layered transition metal dichalcogenides, Chem. Mater. 28 (7) (2016) 1965–1974.

[21] N. M. Renevier, V. C. Fox, D. G. Teer, J. Hampshire, Coating characteristics and tribological properties of sputter-deposited MoS2/metal composite coatings deposited by closed field unbalanced magnetron sputter ion plating, Surf. Coat. Technol. 127 (1) (2000) 24–37.

[22] M. Ye, G. Zhang, Y. Ba, T. Wang, X. Wang, Z. Liu, Microstructure and tribological properties of MoS2+Zr composite coatings in high humidity environment, Appl. Surf. Sci. 367 (2016) 140–146.

[23] P. Stoyanov, R. R. Chromik, D. Goldbaum, J. R. Lince, X. Zhang, Microtribological performance of Au–MoS2 and ti–mos2 coatings with varying contact pressure, Tribol. Lett. 40 (1) (2010) 199–211.

[24] M. C. Simmonds, A. Savan, E. Pflüger, H. Van Swygenhoven, Mechanical and tribological performance of MoS2 co-sputtered composites, Surface and Coatings Technology 126 (1) (2000) 15–24.

[25] T. W. Scharf, R. S. Goeke, P. G. Kotula, S. V. Prasad, Synthesis of au-MoS(2) nanocomposites: thermal and friction-induced changes to the structure, ACS applied materials & interfaces 5 (22) (2013) 11762–11767.

[26] H. Singh, K. C. Mutyala, H. Mohseni, T. W. Scharf, R. D. Evans, G. L. Doll, Tribological performance and coating characteristics of sputter-deposited ti-doped MoS2in rolling and sliding contact, Tribol. Trans. 58 (5) (2015) 767–777.

[27] A. Vellore, S. Romero Garcia, N. Walters, D. A. Johnson, A. Kennett, M. Heverly, A. Martini, Ni-doped MoS $_2$ dry film lubricant life, Adv. Mater. Interfaces 7 (22) (2020) 2001109.

[28] K. Prakash, S. Harish, S. Kamalakannan, T. Logu, M. Shimomura, J. Archana, M. Navaneethan, Perspective on ultrathin layered ni-doped MoS2 hybrid nanostructures for the enhancement of electrochemical properties in supercapacitors, Journal of Energy Chemistry 80 (2023) 335–349.

[29] R. Karkee, E. Guerrero, D. A. Strubbe, Enhanced interlayer interactions in ni-doped MoS2 , and structural and electronic signatures of doping site, Phys. Rev. Mater. 5 (7) (Jul. 2021).

[30] E. Guerrero, D. A. Strubbe, Atomistic mechanisms of sliding in few-layer and bulk doped MoS_2, arXiv [cond-mat.mtrl-sci] (Sep. 2022).

[31] D. Mosconi, P. Till, L. Calvillo, T. Kosmala, D. Garoli, D. Debellis, A. Martucci, S. Agnoli, G. Granozzi, Effect of ni doping on the MoS2 structure and its hydrogen evolution activity in acid and alkaline electrolytes, Surfaces 2 (4) (2019) 531–545.

[32] B. C. Stupp, Synergistic effects of metals co-sputtered with MoS2, Thin Solid Films 84 (3) (1981) 257–266.

[33] H. Wei, Y. Gui, J. Kang, W. Wang, C. Tang, A DFT study on the adsorption of HS and SO on ni doped MoS monolayer, Nanomaterials (Basel) 8 (9) (2018) 646.

[34] M. A. Jenisha, S. Kavirajan, S. Harish, J. Archana, K. Kamalabharathi, E. S. Kumar, M. Navaneethan, Interfacial engineering effect and bipolar conduction of ni- doped MoS2 nanostructures for thermoelectric application, J. Alloys Compd. 895 (162493) (2022) 162493.

[35] J. Zhao, J.-W. Jiang, T. Rabczuk, Temperature-dependent mechanical properties of single-layer molybdenum disulphide: Molecular dynamics nanoindentation simulations, Applied Physics Letters 103 (23) (Dec. 2013).

[36] M. H. Rahman, E. H. Chowdhury, S. Hong, High temperature oxidation of monolayer MoS2 and its effect on mechanical properties: A ReaxFF molecular dynamics study, Surf. Interfaces 26 (101371) (2021) 101371.

[37] J. F. Curry, M. A. Wilson, H. S. Luftman, N. C. Strandwitz, N. Argibay, M. Chandross, M. A. Sidebottom, B. A. Krick, Impact of microstructure on MoS2 oxidation and friction, ACS Appl. Mater. Interfaces 9 (33) (2017) 28019–28026.

[38] M. R. Vazirisereshk, K. Hasz, R. W. Carpick, A. Martini, Friction anisotropy of MoS_2: Effect of tip-sample contact quality, J. Phys. Chem. Lett. 11 (16) (2020) 6900–6906.

[39] Y. Shi, Z. Cai, J. Pu, L. Wang, Q. Xue, Interfacial molecular deformation mechanism for low friction of MoS2 determined using ReaxFF-MD simulation, Ceram. Int. 45 (2) (2019) 2258–2265.

[40] A. Ostadhossein, A. Rahnamoun, Y. Wang, P. Zhao, S. Zhang, V. H. Crespi, A. C. van Duin, ReaxFF reactive force-field study of molybdenum disulfide (MoS2), The journal of physical chemistry letters 8 (3) (2017) 631–640.

[41] I. Ponomarev, T. Polcar, P. Nicolini, New reactive force field for simulations of MoS2 crystallization, The Journal of Physical Chemistry C 126 (22) (2022) 9475–9481.

[42] K. Mohammadtabar, E. Guerrero, S. Romero Garcia, Y. K. Shin, A. C. T. van Duin, D. A. Strubbe, A. Martini, Development and application of a ReaxFF reactive force field for ni-doped MoS_2, J. Phys. Chem. C Nanomater. Interfaces 127 (25) (2023) 12171–12183.

[43] R. Chen, A. Jusufi, A. Schilowitz, A. Martini, Formation of MoS2 from elemental mo and S using reactive molecular dynamics simulations, J. Vac. Sci. Technol. A 38 (2) (2020) 022201.

[44] R. Chen, A. R. Konicek, A. Jusufi, C. E. Kliewer, A. Jaishankar, A. Schilowitz, A. Martini, Limiting domain size of MoS_2: Effects of stoichiometry and oxygen, J. Phys. Chem. C Nanomater. Interfaces 124 (50) (2020) 27571–27579.

[45] M. Taguchi, S. Hamaguchi, MD simulations of amorphous SiO2 thin film formation in reactive sputtering deposition processes, Thin Solid Films 515 (12) (2007) 4879–4882.

[46] M. Taguchi, S. Hamaguchi, Molecular dynamics study on ar ion bombardment effects in amorphous SiO2 deposition processes, J. Appl. Phys. 100 (12) (2006) 123305.

[47] A. A. Gorokh, F. V. Grigoriev, E. V. Katkova, A. V. Sulimov, S. A. Sharapova, High-performance modeling of the deposition of a silicon dioxide thin film using the LAMMPS program, Moscow Univ. Phys. Bull. 71 (1) (2016) 114–117.

[48] F. V. Grigoriev, Force fields for molecular dynamics simulation of the deposition of a silicon dioxide film, Moscow Univ. Phys. Bull. 70 (6) (2015) 521–526.

[49] J. W. Abraham, T. Strunskus, F. Faupel, M. Bonitz, Molecular dynamics simulation of gold cluster growth during sputter deposition, J. Appl. Phys. 119 (18) (2016) 185301.

[50] Z. Ma, F. Duan, Effect of anionic alkyl chain length on tribological properties of ionic liquids: Molecular dynamics simulations, Tribol. Lett. 72 (2) (2024) 1–11.

[51] H. J. C. Berendsen, J. P. M. Postma, W. F. van Gunsteren, A. DiNola, J. R. Haak, Molecular dynamics with coupling to an external bath, J. Chem. Phys. 81 (8) (1984) 3684–3690.

[52] K. Momma, F. Izumi, VESTA 3for three-dimensional visualization of crystal, volumetric and morphology data, J. Appl. Crystallogr. 44 (6) (2011) 1272–1276.

[53] T. Spalvins, Morphological and frictional behavior of sputtered MoS2 films, Thin Solid Films 96 (1) (1982) 17–24.

[54] M. K. Hibbs, B. O. Johansson, J.-E. Sundgren, U. Helmersson, Effects of substrate temperature and substrate material on the structure of reactively sputtered TiN films, Thin Solid Films 122 (2) (1984) 115–129.

[55] J. Moser, F. Lévy, F. Bussy, Composition and growth mode of MoSx sputtered films, J. Vac. Sci. Technol. A 12 (2) (1994) 494–500.

[56] M. R. Hilton, G. Jayaram, L. D. Marks, Microstructure of cosputter-deposited metal- and oxide-MoS2 solid lubricant thin films, J. Mater. Res. 13 (4) (1998) 1022–1032.

[57] E. E. Hoffman, L. D. Marks, Soft interface fracture transfer in nanoscale MoS2, Tribol. Lett. 64 (1) (2016) 1–10.

[58] T. W. Scharf, P. G. Kotula, S. V. Prasad, Friction and wear mechanisms in MoS2/Sb2O3/au nanocomposite coatings, Acta Materialia 58 (12) (2010) 4100–4109.

[59] A. Faiyad, F. H. Bhuiyan, A. Vellore, D. A. Johnson, A. Kennett, A. Martini, Temperature-dependent wear life of MoS*2* dry film lubricants (under review), Tribol. Lett. (2024).

[60] M. A. Hamilton, L. A. Alvarez, N. A. Mauntler, N. Argibay, R. Colbert, D. L. Burris, C. Muratore, A. A. Voevodin, S. S. Perry, W. G. Sawyer, A possible link between macroscopic wear and temperature dependent friction behaviors of MoS_2 coatings, Tribol. Lett. 32 (2) (2008) 91–98.